IOPscience iopscience.iop.org

Home Search Collections Journals About Contact us My IOPscience

Electronic structure and electric field gradients in 2H-TaS_2, $LiTaS_2$ and $SnTaS_2$

This article has been downloaded from IOPscience. Please scroll down to see the full text article.

1991 J. Phys.: Condens. Matter 3 9381

(http://iopscience.iop.org/0953-8984/3/47/011)

View the table of contents for this issue, or go to the journal homepage for more

Download details:
IP Address: 171.66.16.159
The article was downloaded on 12/05/2010 at 10:50

Please note that terms and conditions apply.

J. Phys.: Condens. Matter 3 (1991) 9381–9393. Printed in the UK

Electronic structure and electric field gradients in 2H–TaS_2, $LiTaS_2$ and $SnTaS_2$

P Blaha
Institut für Technische Elektrochemie, Technical University Wien, A-1060 Vienna, Austria

Received 27 June 1991, in final form 22 August 1991

Abstract. The electronic properties of the layered compound 2H–TaS_2 and its Li and Sn intercalates 2H–$LiTaS_2$ and 2H–$SnTaS_2$ are determined from first principles using the full potential linearized augmented plane wave (LAPW) method. Energy band structures, total and partial densities of states, partial charges and electron densities are presented and the bonding mechanism in these compounds is discussed. Using self-consistent electron densities, the electric field gradients (EFG) at all nuclear positions are determined without further approximations and a detailed explanation of the origin of the EFG is given. Good agreement with experimental EFGs is found. From the contact densities at the Ta nuclei, the isomer shifts and a new interpretation of the Mössbauer data for $LiTaS_2$ are presented.

1. Introduction

During the last few years extensive experimental and theoretical investigations of layered transition-metal dichalcogenides have evolved. These compounds change their physical properties rather dramatically upon intercalation with alkali atoms, (post-) transition metals or even inorganic and organic molecules. Structural changes, metal–semiconductor transitions or charge–density waves are observed experimentally. (For a recent review on experimental findings see e.g. Friend and Yoffe 1987.) Besides electron and x-ray diffraction, hyperfine interaction measurements by NMR-, Mössbauer- and TDPAC-spectroscopy have proved to be very effective in the investigation of the different intercalation processes, their dynamics and the resulting structures (Butz *et al* 1986a, Pfeiffer *et al* 1984, Naito *et al* 1986). Such measurements can easily identify atomic sites from the magnitude and asymmetry of the observed electric field gradients (EFG), but the measured quantities are still explained in terms of simple point charge calculations (e.g. Butz *et al* 1986b), where charge transfer effects are only crudely estimated, covalency is completely neglected and which rely on the validity of atomic Sternheimer antishielding factors.

Recently, Blaha *et al* (1985) developed a first-principles approach to calculate the EFG. This method is based on accurate energy band structure calculations from which the EFG is computed directly using the resulting total charge density of the crystal. Since all electrons are included in such self-consistent calculations, Sternheimer antishielding, charge transfer and covalency effects are fully taken into account, as long as the electronic structure calculation is performed with high accuracy and the underlying local density

0953-8984/91/479381 + 13 $03.50 © 1991 IOP Publishing Ltd

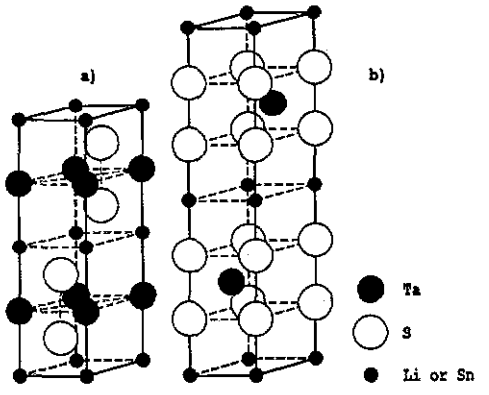

Figure 1. Hexagonal unit cell of (*a*) 2H–(Li)TaS_2 and (*b*) $SnTaS_2$.

approximation (LDA) for treating exchange and correlation holds. This method was applied successfully to systems with different bonding characteristics like the HCP metals (Blaha *et al* 1988), to insulators like Li_3N (Blaha *et al* 1985) or Cu_2O (Blaha and Schwarz 1989), or to various high temperature superconductors (Schwarz *et al* 1990, Ambrosch-Draxl *et al* 1991).

Here we will concentrate on 2H–TaS_2 and two simple intercalates, namely $LiTaS_2$ and $SnTaS_2$, which have been thoroughly investigated experimentally (Butz and Lerf 1982, Friend and Yoffe 1987) and might serve as prototype materials for the layered dichalcogenide family. In particular we will focus on the changes in the electronic structure upon alloying, making a comparison with the rigid-band model and explain in detail the origin of the EFG in these compounds.

2. Crystal structures and computational details

TaS_2 exists in several polytypes, but here we investigate only the modification that is stable at room temperature, namely 2H–TaS_2. It belongs to the hexagonal non-symmorphic space group $P6_3/mmc$, in which the Ta and S atoms occupy positions 2b and 4f (with $z = 1/8$), respectively (Jellinek 1962). This structure (figure 1(*a*) without Li) consists of two hexagonal double layers of S atoms, between which the Ta atoms occupy the trigonal-prismatic holes forming another hexagonal layer. The individual S–Ta–S layers are displaced by 1/3 in the *a* and *b* directions resulting in a AcA–BcB stacking along the *c* axis.

Fully intercalated 2H–$LiTaS_2$ shows almost no change in the structural parameters (Murphy *et al* 1976), but the exact Li position is difficult to determine since Li has a low x-ray scattering intensity relative to Ta (or S). It is generally believed that Li occupies the octahedral sites, namely position 2a (figure 1(*a*)). So far the *z* parameter of the S position could not be determined experimentally, but we have determined this parameter theoretically by means of total energy calculations.

Intercalation with Sn has a larger effect on the crystal structure. Although the space group remains the same, the *c* axis increases by about 50% and the stacking sequence of the S–Ta–S layers changes from AcA–BcB to AcA–AcA (Eppinga and Wiegers 1977). Figure 1(*b*) shows the Sn atoms (position 2a), which are linearly coordinated by S (position 4e with $z = 0.16$) while here the Ta atoms occupy position 2c. This structure

is much more open than $LiTaS_2$ and reflects the different size and character of Li and Sn ions.

We performed self-consistent linearized augmented plane wave (LAPW) energy band structure calculations based on the local density approximation. We use the WIEN code (Blaha *et al* 1990), which utilizes a general potential and thus avoids the common muffin-tin approximation, which would be inaccurate for such anisotropic structures. Scalar-relativistic effects are included and a basis set of about 400–500 plane waves is used. Brillouin zone integrations and densities of states (DOS) calculations are performed with a tetrahedron method using 148 $\boldsymbol{k}$ points in the irreducible wedge. The semi-core states (Li–1s and Ta–5s, 5p) are treated in a separate energy window as band-like states, while the lower core states are recalculated every iteration in the spherical part of the potential (thawed core).

The general expression for the principal component of the EFG arising from a charge density $\rho(r)$ is defined as

$$V_{zz} = \int \rho(r)\, 2P_2(\cos\theta)/r^3 \, \mathrm{d}r \tag{1}$$

where P_2 is the second-order Legendre polynomial. We now use for $\rho(r)$ the self-consistent total charge density of our LAPW calculations and obtain the EFG at the various atomic sites directly from first principles without making assumptions on different ionicities or applying atomic Sternheimer anti-shielding factors. Details of the EFG calculations can be found in Blaha *et al* (1985 and 1988) or Schwarz *et al* (1990).

3. Energy band structures and density of states

Besides several semi-empirical studies the non-self-consistent band calculations by Mattheiss (1973) provided the first insight into the electronic structure of layered transition-metal-dichalcogenides. For 2H–TaS_2 and some of its intercalates Guo and Liang (1987) and Dijkstra *et al* (1989) performed self-consistent calculations with the linear-muffin-tin-orbital (LMTO) and augmented-spherical-wave (ASW) method respectively. However, both calculations used the atomic sphere approximation (ASA), which could be responsible for some of the differences between their results.

In figures 2–4 we show the band structures and DOS of TaS_2, $LiTaS_2$ and $SnTaS_2$. For the bands in TaS_2 (figure 2) we give a detailed description below: the lowest four bands (around −0.5 Ry) originate from S–s states; bands ranging from 0.0 to 0.4 Ry are the S–p bands (with an appreciable amount of Ta–d character) and the two half-filled bands around the Fermi-energy (E_F) will be called Ta–d_{z^2} bands, although we will show later that there is additional S–p and—in particular—also a (Ta–d_{xy}, $d_{x^2-y^2}$) admixture. The overall agreement with the band structure by Guo and Liang (1987) is very good (in particular the occupied part), while pronounced differences occur to the ASW results (Dijkstra *et al* 1989). Probably, this is because the latter authors did not try to improve the ASA approximation by introducing additional empty spheres, while in the LMTO calculations empty spheres at positions 2a (the Li–site in $LiTaS_2$) are used. The main differences are a much stronger indirect overlap between the S–p and the Ta–d_{z^2} band (mainly at Γ) and a somewhat smaller bandwidth of 6.2 eV versus 6.8 eV for the total width from the bottom of the S–p bands to E_F. We find an indirect gap of 0.4 eV from Γ to K between the Ta–d_{z^2} and higher Ta–d bands, while both ASA calculations obtain a

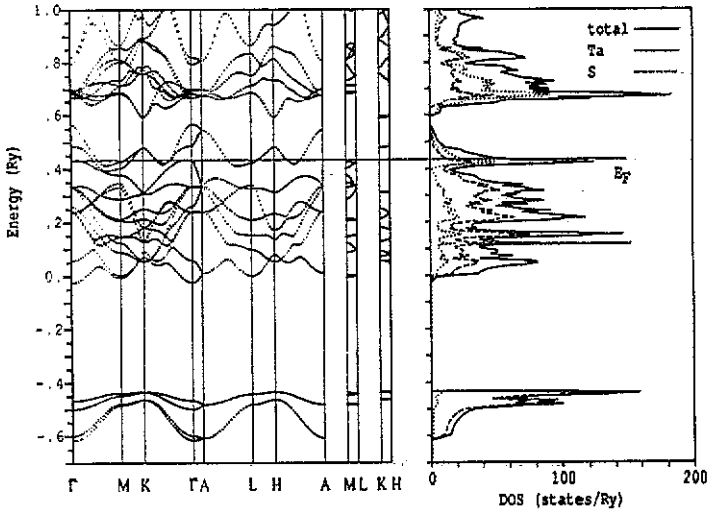

Figure 2. Energy band structures and density of states (DOS) for TaS_2.

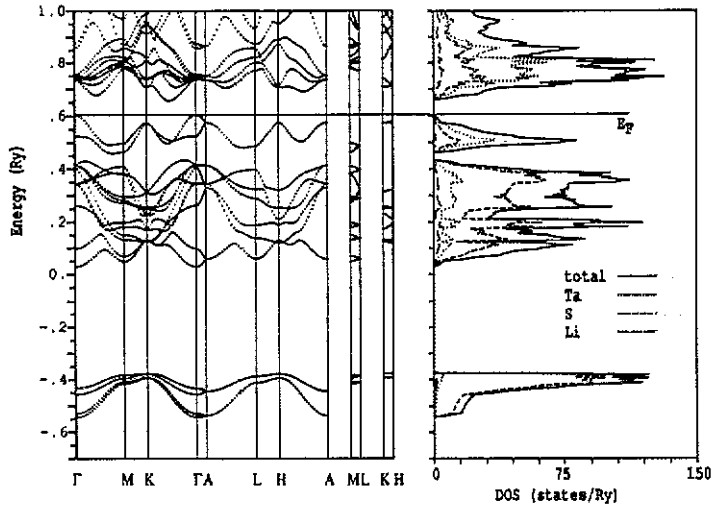

Figure 3. Energy band structures and density of states (DOS) for $LiTaS_2$.

gap of more than 1 eV. Nevertheless, the agreement between all self-consistent calculations is quite good, while large differences to the non-self-consistent calculations by Mattheiss (1973) are evident. The partial DOS corroborate the assignments given above. The Fermi energy clearly falls above the maximum of the Ta–d_{z^2} peak and we obtain a DOS at E_F of 5.0 states eV^{-1}/cell, very similar to the value of 5.2 quoted by Guo and Liang, and in good agreement with experimental estimates (DiSalvo *et al* 1971).

In $LiTaS_2$ (figure 3) the Ta–d_{z^2} bands are filled due to the two additional electrons (coming from Li 2s) and an insulator with a gap of about 0.7 eV is found. The Ta–d_{z^2} bandwidth is decreased upon Li intercalation and these bands are separated from the

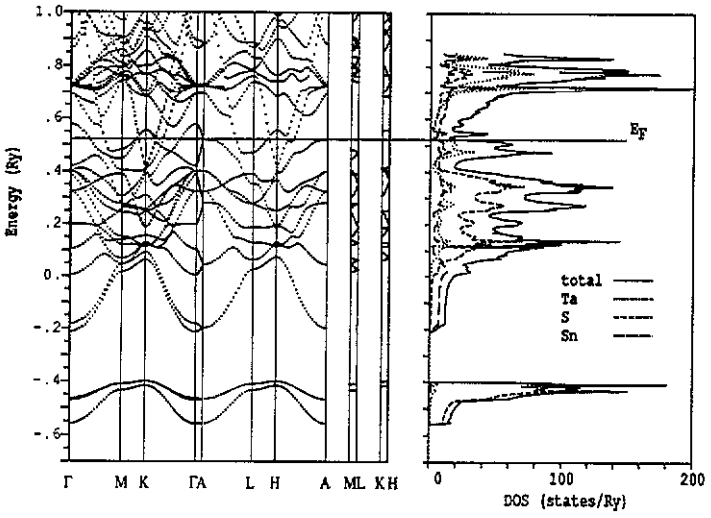

Figure 4. Energy band structures and density of states (DOS) for $SnTaS_2$.

lower lying S–p bands by 0.3 eV. These two Ta–d_{z^2} bands are therefore most affected, but there is also some rearrangement in the S–p bands. (See also the discussion in chapter 4.)

The band structure of $SnTaS_2$ (figure 4) is more complicated than the ones discussed above, since we have additional Sn states which mix with all other bands. The Ta–d_{z^2} bands are almost filled as can be seen from the partial Ta–DOS, which drops sharply at E_F, but the metallic character remains since several bands (mainly of Sn–p character) cross E_F. In order to provide more information on the nature of certain energy bands, we repeat part of the $SnTaS_2$ band structure in figure 5, where each state is weighted by the Sn partial charge: the small dots in figure 5 correspond to Sn-free states, while the large circles indicate the predominant Sn character of that particular eigenvalue. In this representation it is easy to identify the Sn–s bands (ranging from −0.2 to 0.1 Ry) and the bands with strong Sn–p character (starting at M around 0.3 Ry). Large differences occur to the energy bands of both ASA calculations, probably since the ASA shape approximation is too crude for this structure, which is even more anisotropic than pure TaS_2.

4. Partial charges, charge densities and chemical bonding

In table 1 the Ta and S partial charges are listed. These values are obtained from an integration of the $l(m)$-like charge density over the respective atomic sphere (with a radius of 2.3 au in both cases). This corresponds to a spatial decomposition of the electronic charge and since delocalized wavefunctions are only partly confined to the atomic spheres, a lot of charge lies outside the spheres and thus cannot be analysed further. Therefore, one must be careful in the interpretation of these partial charges and, in particular, in estimates of charge transfer and ionicity. They are, however, quite valuable when we compare a series of related compounds as in table 1. Three columns are given for $LiTaS_2$: in the first two the z-values of the S-position are varied, where a

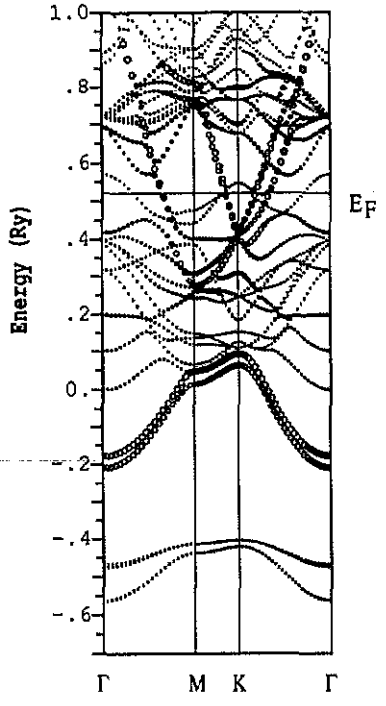

Figure 5. Part of the energy band structure of $SnTaS_2$. The size of the circles is proportional to the Sn partial charge of the respective band state.

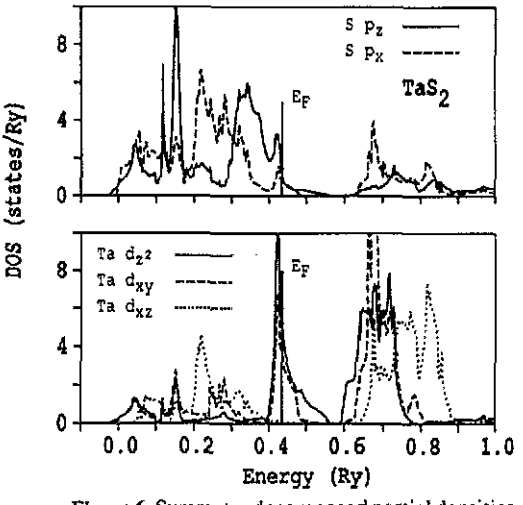

Figure 6. Symmetry decomposed partial densities of states (DOS) for TaS_2. The top panel shows the sulphur, the bottom panel the Ta DOS.

Table 1. Partial charges (in electrons) in TaS_2, $SnTaS_2$ and three different $LiTaS_2$ calculations (see text); z corresponds to the S z-position.

	TaS_2	$SnTaS_2$	$LiTaS_2$ $z = 0.127$	$LiTaS_2$ $z = 0.130$	$LiTaS_2$ Rigid
Ta–s	0.212	0.198	0.191	0.195	0.218
Ta–p	0.220	0.200	0.196	0.204	0.225
Ta–d	2.026	2.039	2.061	2.093	2.455
Ta–p_z	0.081	0.071	0.070	0.073	0.082
Ta–p_{xy}	0.139	0.129	0.126	0.131	0.143
Ta–d_{z^2}	0.349	0.455	0.486	0.491	0.552
Ta–d_{xy}	0.773	0.811	0.856	0.863	0.997
Ta–d_{xz}	0.904	0.773	0.720	0.738	0.906
S–s	1.621	1.607	1.593	1.593	1.627
S–p	3.141	3.164	3.253	3.264	3.238
S–p_z	1.091	1.050	1.107	1.114	1.134
S–p_{xy}	2.050	2.114	2.146	2.150	2.104

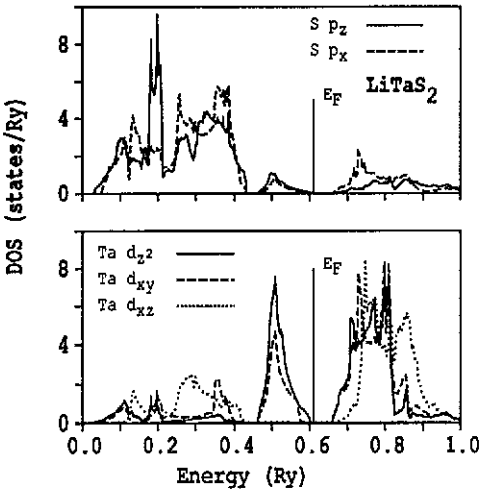

Figure 7. Symmetry decomposed partial densities of states (DOS) for $LiTaS_2$ (see figure 6).

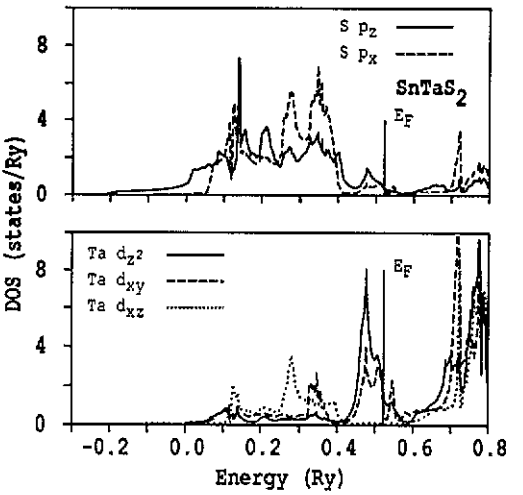

Figure 8. Symmetry decomposed partial densities of states (DOS) for $SnTaS_2$ (see figure 6).

larger z-value corresponds to shorter S–S and Ta–S, but to longer Li–S distances; the third column, termed 'rigid', corresponds to a rigid band model in which the effect of the additional electron from Li is simulated by just moving up the Fermi energy in the band structure of pure TaS_2, assuming that it remains rigid upon Li intercalation.

Starting with TaS_2 and a very simple ionic picture one would expect the S–p bands to be fully occupied with six electrons, while the Ta^{4+} ion would have only one remaining d-electron. Obviously, this picture neglects all other bonding effects and we see already from the partial DOS in figures 2–4 (and 6–8) that in the so-called S–p band an appreciable admixture of Ta–d states exists. In addition, we find more than two d-electrons inside the Ta sphere of TaS_2, indicating strong covalent interactions and less ionic bonding. If we compare the charges across the series in table 1 we find surprisingly similar values for the Ta–s, p and d- partial charges, only the 'rigid' $LiTaS_2$ result shows a large charge transfer to the Ta site as one would expect from a rigid-band picture. Doping of TaS_2 with Li or Sn apparently does not increase the total charge in the Ta sphere. This can be understood by examining the Ta partial charges of the S–p and the Ta–d_{z^2} bands separately. In the series TaS_2, $SnTaS_2$ and $LiTaS_2$ ($z = 0.127$) there is a decrease of the Ta–d charge in the S–p band from 1.66 to 1.42 and 1.25 respectively (similar, but less pronounced for s- and p-charges), but this decrease is compensated by an increased Ta–d charge in the (now filled) Ta–d_{z^2} band. This explains why Li (Sn) intercalation does not increase the Ta charge but leads to a more ionic bond between Ta and S. This change in bonding character is consistent with the increasing S–Ta distances upon intercalation and the separation of the Ta–d_{z^2} bands from the S–p bands in $LiTaS_2$ (figure 3). The S p-charge increases only slightly, since a large fraction of it is outside the S sphere and an additional S charge will enhance the delocalization of the p-wavefunctions reducing the charge inside the S sphere.

The total Ta–d charge is not changed upon intercalation, but the anisotropy of the Ta–d charge is altered. The Ta–d_{xz}, d_{yz} (in short only d_{xz}) orbitals dominate in the S–p band (see bottom of figure 6) and form covalent bonds with the S–p_x, p_y (in short p_x) orbitals. This interaction is strongest in TaS_2 but decreases in $SnTaS_2$ and $LiTaS_2$ (table

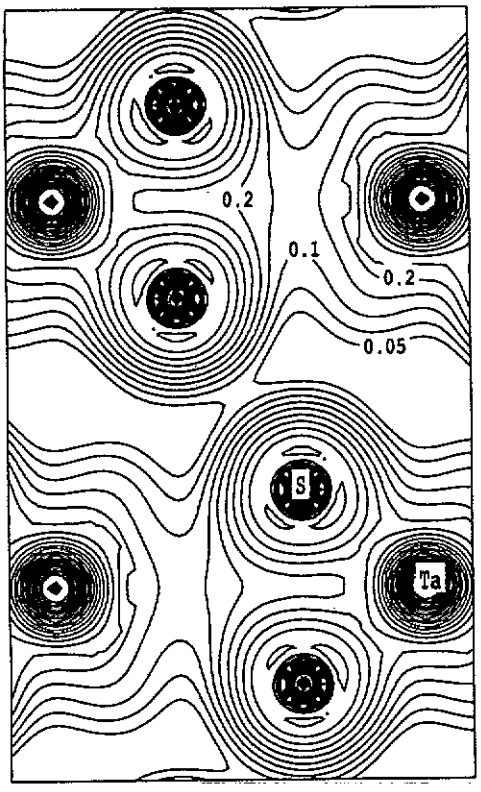

Figure 9. Valence charge density of TaS_2 in the $(11\bar{2}0)$ plane. Contours differ by a factor of $\sqrt{2}$, the numbers are in units of e $Å^{-3}$.

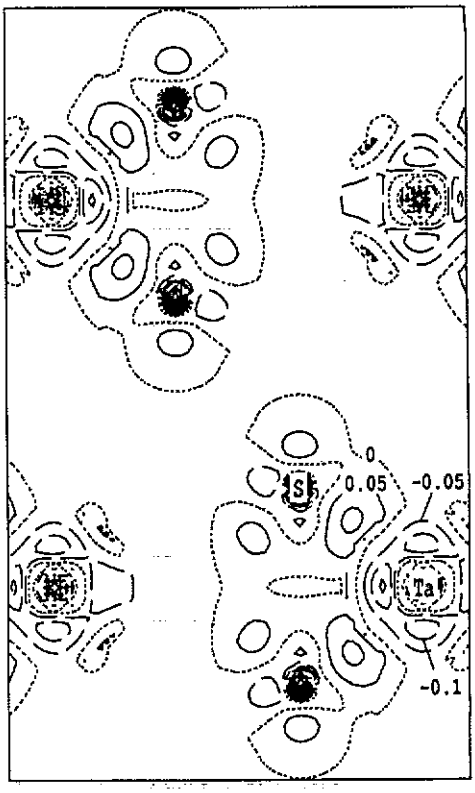

Figure 10. Difference electron density of TaS_2 between the crystal and a density of superposed neutral atoms. Adjacent contours differ by 0.05 e $Å^{-3}$; zero is indicated by short dashed lines, negative contours are indicated by long dashed lines.

1). The other two symmetry components are much smaller in TaS_2, but increase as the Ta–d_{z^2} band is filled. Note that the so-called d_{z^2} band has, in addition, a large d_{xy}, $d_{x^2-y^2}$ (in short d_{xy}) component (figures 6–8) and also some S–p admixture. In TaS_2 this admixture is predominantly of p_z character, since the S–p_z DOS is shifted to higher energies and separated from the S–p_x DOS (figure 6), while in $LiTaS_2$ and $SnTaS_2$ the S–p admixture in the Ta–d_{z^2} band is greatly reduced and in the S–p band the p_z and p_x partial density of states falls in the same energy range (figures 7 and 8).

Next, the charge density is examined in real space. The valence charge density (including the Ta 4f states) shown in figure 9 gives a clear impression of the layered structure and the chemical bonding in these compounds. The density in the TaS_2 slab is quite high and covalent contributions can be seen from the charge maxima of the S–p density pointing towards the Ta site. The density between the slabs is relatively low and the distance between two slabs is determined by the S–S contact. The asphericity of the charge distribution around both sites as well as the charge transfer can better be seen in the difference electron densities (figure 10), where overlapping neutral atomic charge densities are subtracted from the crystalline density. Negative difference densities

Table 2. Theoretical and experimental EFGs in TaS_2, $SnTaS_2$ and $LiTaS_2$ (in units of 10^{18} V cm^{-2}). The two experimental values for the Ta–EFG refer to the same experiment, but to different ^{181}Ta(5/2) quadrupole moments (Butz and Lerf 1983), $Q = 2.36$b (the more recent Q) or the older value of $Q = 2.8$b (EFGs in parentheses). The theoretical $LiTaS_2$ results refer to a calculation with an S z-coordinate of 0.127 except in the line specifically indicated.

		Theory	Experiment
2H–TaS_2	Ta	−1.43	−1.62, (−1.36)†
	S	−0.46	
$SnTaS_2$	Ta	−0.73	−1.08, (−0.91)‡
	S	+0.12	
	Sn	+1.54	+1.80§
$LiTaS_2$	Ta	−0.39	−0.66, (−0.56)‖
			−0.46, (−0.39)¶
($z = 0.130$)	Ta	−0.54	
	S	−0.21	
	Li	−0.0057	±0.0054††

† Butz and Lerf (1982), extrapolated to 0 K.
‡ Butz *et al* (1987), extrapolated to 0 K.
§ Herber and Davis (1976), extrapolated to 0 K. (^{119}Sn $Q = -0.094$b).
‖ Butz and Lerf (1982).
¶ Eibschütz *et al* (1988), extrapolated to 0 K.
†† Silbernagel (1975).

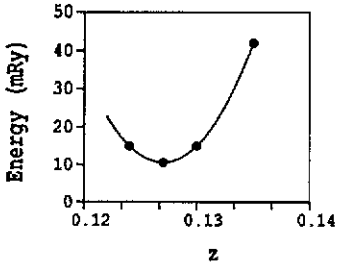

Figure 11. Total energy (arbitrary absolute scale) versus sulphur z-coordinate in $LiTaS_2$.

around Ta and positive ones around S indicate a charge transfer from Ta to S. When the densities of charged ions instead of neutral atoms are subtracted, we estimate from the residual difference densities that Ta loses less than one d electron and S gains about 0.5–1.0 p-electrons. It is impossible to give a more precise estimate about the absolute charge transfer. Note that independent of the assumed ionicities of the subtracted ions, a negative difference density between the slabs and a positive one within the slabs occurs indicating a charge accumulation in the TaS_2 slabs.

5. Electric field gradients and isomer shifts

The EFGs are calculated for all possible sites and are listed in table 2 together with the available experimental values. The measured quadrupole frequency depends on the

Table 3. 5p-semicore and valence (4f, 5d, 6s, 6p) contributions to the total EFG at the Ta site in TaS_2, $SnTaS_2$ and $LiTaS_2$ (in 10^{18} V cm^{-2}).

	Total	Semicore	Valence
TaS_2	−1.43	+0.03	−1.44
$SnTaS_2$	−0.73	+0.12	−0.85
$LiTaS_2$ ($z = 0.127$)	−0.39	+0.30	−0.70
$LiTaS_2$ ($z = 0.130$)	−0.54	+0.25	−0.79
$LiTaS_2$ ('rigid')	−1.15	+0.03	−1.18

product of the EFG times the nuclear quadrupole moment Q, and since two values for Q are available from literature (Butz and Lerf 1983), we quote two 'experimental' values for the EFGs at the Ta site, which are obtained from the same experiment, but with different values for Q. (Note that $Q = 2.36$ b for ^{181}Ta(5/2) is the more recent value.) Given these uncertainties in Q the agreement between theory and experiment is rather good.

In $SnTaS_2$ the EFGs at the Ta and Sn sites have been measured and good agreement is found between theoretical and experimental EFGs. The Ta EFG is reduced by a factor of two upon intercalation.

Two complications arise for $LiTaS_2$, namely that the z-coordinate of the S-position is not known experimentally and that the results of TDPAC measurements (Butz and Lerf 1982) and Mössbauer spectroscopy (Eibschütz *et al* 1988) do not agree well with each other. In the present investigation we find that the EFG at the Ta site is extremely sensitive to the z-position of the S atom (table 2). In order to eliminate this uncertainty we performed total energy calculations as a function of the S z-coordinate (figure 11). We found an energy minimum at $z = 0.127$, which is exactly the value one obtains when the c axis expansion upon Li intercalation is distributed equally between the inter- and intra-sandwich heights. When this equilibrium z-value for the S position is used, the theoretical EFG at the Ta site is relatively low compared with experiment, but the large differences among the experimental data could indicate difficulties in the sample preparation. The EFG at the Li site has been measured too. It is extremely small (as expected for a Li^+-ion) and agrees perfectly well between theory and experiment.

Table 3 gives an analysis of the different contributions to the Ta-EFG. As in other systems studied before (Blaha *et al* 1985, 1988, Blaha and Schwarz 1989) the EFG stems mostly from contributions inside the respective atomic sphere, while the part from the outside region is almost negligible. This is because the factor $1/r^3$ enters the EFG calculation and weights the non-spherical charge density, see (1). The latter can be split into contributions from semicore (Ta 5s and 5p) and valence states. It is interesting to note that the semicore contribution is very small for pure TaS_2, but it makes a substantial part of the EFG for the intercalated compounds. A weak interaction of the Ta–5p states with the neighbouring Li atoms leads to an anisotropy of the 5p charge distribution, where the p_z occupation is smaller than $p_{x(y)}$ by about 0.001 electrons. Although this *difference in occupation numbers is very small, it nevertheless gives a substantial* EFG contribution due to the large $\langle r^{-3} \rangle$ expectation value of the 5p orbital.

The valence EFG can be split further into p–p and d–d contributions (Blaha *et al* 1988), while additional s–d and higher l-components are negligible (except for 'rigid'

Table 4. p–p and d–d contributions to the valence Ta–EFG (in 10^{18} V cm^{-2}), asymmetry counts Δn_p and Δn_d and average $\langle r^{-3}\rangle$ expectation values (in au^{-3}) for Ta 5d and 6p wavefunction.

	EFG_{p-p}	Δn_p	$\langle r^{-3}\rangle_p$	EFG_{d-d}	Δn_d	$\langle r^{-3}\rangle_d$
TaS_2	−1.34	−0.0125	110	−0.10	−0.0285	4
$LiTaS_2$	−0.79	−0.0075	108	+0.08	+0.0095	9
$LiTaS_2$ (rigid)	−1.11	−0.0110	104	−0.01	−0.0080	2

$LiTaS_2$, where an unusully large s–d contribution of $-0.06\,10^{18}$ V cm^{-2} is found). In this simplification the valence EFG can be written as

$$V_{zz}^{val} = \Delta n_p \langle r^{-3}\rangle_p + \Delta n_d \langle r^{-3}\rangle_d \tag{2}$$

where $\langle r^{-3}\rangle$ is an averaged expectation value of the respective orbitals and the asymmetry counts Δn_p and Δn_d are defined in terms of symmetry decomposed partial charges as

$$\left.\begin{aligned} \Delta n_p &= 1/2(p_x + p_y) - p_z \\ \Delta n_d &= (d_{xy} + d_{x^2-y^2}) - 1/2(d_{xz} - d_{yz}) - d_{z^2}. \end{aligned}\right\} \tag{3}$$

We find that the asymmetry counts Δn_p and Δn_d are comparable in magnitude (table 4), but for the EFG the p–p part dominates over the d–d part owing to its larger $\langle r^{-3}\rangle$ expectation value. The small 6p charges, which probably originate from a re-expansion of the tails of S–p wavefunctions entering the Ta sphere, are much more aspherically distributed than the larger 5d contributions with a fairly small asymmetry count Δn_d. The latter is small although the individual symmetry decomposed d contributions differ substantially (table 1). The $\langle r^{-3}\rangle_p$ expectation values are about constant indicating only a small energy dependence, while the d-expectation values vary a lot among the examples presented in table 4, as will be explained below.

It is often thought that the rigid band model is applicable to $LiTaS_2$, since the Li should be totally ionized and its electron should simply be accommodated in the half-filled TaS_2 Ta–d_{z^2} band. However, in such a rigid band calculation for $LiTaS_2$ we obtain an EFG which is far too large (table 4). This confirms our results discussed in the previous sections, where we have explained that a rigid band model is not applicable to $LiTaS_2$, since Li intercalation causes the Ta–S bond to become more ionic. In going from TaS_2 to 'rigid' TaS_2 we occupy additional Ta–d states at higher energy, which are more delocalized, so that the average of the $\langle r^{-3}\rangle_d$ value decreases. In the actual $LiTaS_2$ calculations, however, we have a much more ionic bond and thus more localized d-wavefunctions yielding a larger $\langle r^{-3}\rangle_d$.

Another argument for a simple charge transfer (rigid-band) model of the intercalated TaS_2 compounds comes from Mössbauer measurements by Eibschütz *et al* (1988), who found that the isomer shift (IS) is directly proportional to the Li content. The IS is given by

$$IS = \alpha[\rho(0) - \rho_{ref}(0)] \tag{4}$$

where $\rho(0)$ is the contact density at the nucleus and α is the nuclear calibration constant, which depends only on the nuclear states involved in the Mössbauer measurement. Since, in the experiment mentioned above, BCC Ta was used as a reference, we performed a band structure calculation for that reference system. The contact densities for BCC Ta,

Table 5. Total and partial contact densities and $\Delta\rho(0) = [\rho(0) - \rho_{ref}(0)]$ (taken at a fixed distance of 5×10^{-5} au from the nucleus) at the Ta site *in* BCC Ta, TaS_2, $SnTaS_2$ and $LiTaS_2$.

	Valence	Semicore	Core	Total	$\Delta\rho(0)$
BCC Ta	119.9	1945.8	1698612.6	1700678.3	0.0
TaS_2	97.5	1945.6	1698613.6	1700656.7	−21.6
$SnTaS_2$	90.8	1946.0	1698613.9	1700650.7	−27.6
$LiTaS_2$	88.3	1945.7	1698613.9	1700647.9	−30.4

TaS_2, $LiTaS_2$ and $SnTaS_2$ are given in table 5. From these values together with the experimental IS of TaS_2 (70.26 mm s^{-1}) we extract a nuclear calibration constant $\alpha = -3.25\, a_0^3$ mm s^{-1} and obtain with this α an IS for $LiTaS_2$ of 98.9 mm s^{-1}, which is in perfect agreement with the experimental value of 100 mm s^{-1}. A somewhat smaller shift of 89.8 mm s^{-1} is obtained for $SnTaS_2$. These results, however, lead to a different interpretation than the one given in the experimental paper, where a simple relation 'large IS—large charge transfer to Ta' is claimed. The present calculations show that almost no charge transfer is found and the Ta contact density decreases in the series BCC Ta, TaS_2, $SnTaS_2$ and $LiTaS_2$, yielding a negative α. This trend can be understood considering that a metal usually has more of its valence s electrons (conduction electrons, 'electron gas'), than an ionic compound such as TaS_2, so that the latter has lost some of its 6s electrons and thus has a smaller contact density. Apparently, in $LiTaS_2$ the Ta atom has even less 6s electrons, since—as interpreted before—Li intercalation increases the ionicity of the Ta–S bond, but does not transfer s electrons to the Ta sites.

6. Summary

We have performed energy band structure calculations for 2H-TaS_2 and two of its intercalates, namely $LiTaS_2$ and $SnTaS_2$ using the full potential LAPW method. Our calculations are in fair agreement with previous self-consistent calculations, but we avoid here the commonly used atomic sphere approximation, which could lead to inaccuracies for such anisotropic crystal structures. The chemical bonding in this class of materials is partly ionic, but covalent contributions are important too. Intercalation with Li is often described within a rigid bond model, where the Li 2s electron is simply accommodated in the Ta–d_{z^2} band forming an insulating compound. We found that Li intercalation weakens the covalent interaction and increases the ionicity of the S–Ta bond, so that this compensation leads to an almost identical total charge at the Ta site. Calculated electric field gradients and isomer shifts are in good agreement with experiment and support the picture of the chemical bonding given above.

Acknowledgments

I am grateful for several stimulating discussions with Dr T Butz and Dr A Lerf and to Prof K Schwarz for his continuous support of this work. Computations were performed on the IBM 3090-400 VF of the University of Vienna Computer Centre within the European Academic Supercomputer Initiative (EASI) sponsored by IBM.

References

Ambrosch-Draxl C, Blaha P and Schwarz K 1991 *Phys. Rev.* B **44** 5141
Blaha P and Schwarz K 1989 *Hyperfine Interact.* **52** 153
Blaha P, Schwarz K and Dederichs P H 1988 *Phys. Rev.* B **37** 2792
Blaha P, Schwarz K and Herzig P 1985 *Phys. Rev. Lett.* **54** 1192
Blaha P, Schwarz K, Sorantin P and Trickey S B 1990 *Comp. Phys. Commun.* **59** 399
Butz T, Ebeling K H, Hagn E, Saibene S, Zech E and Lerf A 1986a *Phys. Rev. Lett.* **56** 639
Butz T, Klapp U and Lerf A 1987 *Chemical Physics of Intercalation* ed A P Legrand and S Flandrois (Plenum) p 403
Butz T and Lerf A 1982 *Rev. de Chimie Minerale* **19** 496
—— 1983 *Phys. Lett.* **97A** 217
Butz T, Saibene S and Lerf A 1986b *J. Phys. C: Solid State Phys.* **19** 2675
Dijkstra J, Broekhuisen E A, van Bruggen C F, Haas C, deGroot R A and van der Meulen H P 1989 *Phys. Rev.* B **40** 12111
DiSalvo F J, Schwall R, Geballe T H, Gamble F R and Osiecki J H 1971 *Phys. Rev. Lett.* **34** 310
Eibschütz M, Salomon D, Zahurak S and Murphy D W 1988 *Phys. Rev.* B **37** 3082
Eppinga R and Wiegers G A 1977 *Mater. Res. Bull.* **12** 1957
Friend R H and Yoffe A D 1987 *Adv. Phys.* **36** 361
Guo G Y and Liang W Y 1987 *J. Phys. C: Solid State Phys.* **20** 4315
Herber R H and Davis R F 1976 *J. Chem. Phys.* **65** 3773
Jellinik F 1962 *J. Less-Common Met.* **4** 9
Mattheiss L F 1973 *Phys. Rev.* B **8** 3719
Murphy N M, DiSalvo F J, Hull G W Jr and Waszczak J V 1976 *Inorg. Chem.* **15** 17
Naito M, Nishihara H and Tanaka S 1986 *J. Phys. Soc. Japan* **55** 2410
Pfeiffer L, Kovacs T and DiSalvo F J 1984 *Phys. Rev. Lett.* **52** 687
Schwarz K, Ambrosch-Draxl C and Blaha P 1990 *Phys. Rev.* B **42** 2051
Silbernagel B G 1975 *Solid State Commun.* **17** 361